Research Article | Vol. 11, No. 7 / 1 July 2020 / Biomedical Optics Express 3534
Biomedical Optics EXPRESS

Stepped frequency comb generation based on electro-optic phase-code mode-locking for moderate-speed circular-ranging OCT

TAE SHIK KIM[1,2,*] AND BENJAMIN J. VAKOC[1,2]

[1]Harvard Medical School, Boston, Massachusetts 02115, USA
[2]Wellman Center for Photomedicine, Massachusetts General Hospital, Boston, Massachusetts 02114, USA
[*]tkim22@mgh.harvard.edu

Abstract: Circular-ranging (CR) optical coherence tomography (OCT) uses frequency comb sources to improve long-range imaging. While the initial development of CR-OCT focused on extremely high-speed imaging (i.e., operation at A-line rates of several to tens of MHz), there are many applications and imaging strategies for which more moderate speeds are preferred. However, we lack suitable frequency comb sources to enable moderate speed CR-OCT imaging. Here, we describe a novel phase-code mode-locking (PCML) laser architecture that can be operated from the kilohertz to megahertz range, while also offering novel features such as dynamic re-configurability and simplified linear-in-time frequency stepping. We demonstrate a prototype CR-OCT system with a PCML laser and present imaging results at A-line rates from 176 kHz to 3.52 MHz with coherence-length limited imaging depths as high as 170 mm.

1. Introduction

Optical coherence tomography (OCT) is a widely used three-dimensional imaging modality defined by its use of echo-delay depth ranging [1,2]. In recently described circular-ranging (CR) OCT methods, stepped-in-time frequency comb sources were used to enable compressive echo-delay ranging. With compressive ranging, fewer measurements are required to interrogate long depth ranges. This reduces the bandwidth requirements of the electronics used to capture and process the output signals [3]. Using high-speed stepped frequency comb sources based on stretched-pulse mode-locking (SPML) [4], CR-OCT was demonstrated at speeds in excess of 10 MHz [5,6].

The compression provided by CR can also be used to reduce electronic bandwidth requirements in more moderate speed, long-range imaging applications. Unfortunately, the SPML laser is poorly suited to moderate speed imaging; a prohibitively long chirped fiber Bragg gratings would be required to reduce speeds below several megahertz. Moderate speed CR-OCT has instead relied on sources created by modifying existing swept-source laser architectures. Fixed Fabry-Pérot etalons have been added to polygon-mirror and micro-mechanical Fabry-Perot swept-wavelength lasers [3,7,8]. While this yields the required stepped frequency comb output, the noise and coherence length properties have been relatively poor and the nonlinear-in-time output pulse sequence complicates signal capture.

In this work, we describe a novel stepped frequency comb laser architecture for use in CR-OCT. This laser architecture is termed phase-code mode-locking (PCML). Like the SPML laser, the PCML laser uses intracavity dispersion and electro-optic modulation instead of mechanically-tuned spectral filters. The key difference between SPML and PCML architectures is that the former uses electro-optic amplitude modulation, while the later uses electro-optic phase modulation. This distinction is important because it allows the laser repetition rate to be decoupled from the intracavity dispersion. As a result, the PCML laser is able to operate at moderate speeds using reasonable levels of intracavity dispersion. Moreover, a PCML source can be operated over a

#392359 https://doi.org/10.1364/BOE.392359
Journal © 2020 Received 9 Mar 2020; revised 7 May 2020; accepted 8 May 2020; published 8 Jun 2020

Biomedical Optics EXPRESS

wide-range of speeds without hardware modification, and a nearly arbitrary combline sequence (i.e., order of output wavelengths in time) can be generated.

In Section 2, we describe the PCML laser principles. Section 3 describes a prototype PCML, and Section 4 demonstrates its performance across a speed-range of 176 kHz to 3.52 MHz at 1550 nm with 80 nm of optical bandwidth and a coherence-length limited imaging range that varied from 100 to 170 mm depending on the specific configuration. Additionally, we present in Section 4 proof-of-principle PCML-based CR-OCT imaging results.

2. PCML laser operating principle

The PCML laser leverages reversible electro-optic linewidth broadening to create a frequency combline transmission filter. This principle is relatively straightforward and is illustrated in Fig. 1. As a starting point, we first analyze the evolution of a narrowband, CW input field at optical frequency ω and described by $E_A(t) = \cos(\omega t)$ that passes through two sequential phase modulators (Fig. 1(a)). Light is launched at point A. The first modulator is driven by a voltage drive signal $f_1(t)$, resulting in an output field given by $E_B(t) = \cos(\omega t + \alpha f_1(t)))$ where α is the modulator's scale-factor between induced phase shift and drive voltage (rad/V). For simplicity, we assume that α is a constant across RF frequency and optical frequency.

This phase modulation broadens the linewidth of the light at point B, as illustrated in Fig. 1(a). The spectrally-broadened light travels to the second phase modulator located a distance d (in fiber, point C) from the first modulator. The field at this point is given by $E_C(t) = \cos(\omega(t - dn/c) + \alpha f_1(t - dn/c))$ where n is the group index of the fiber and c is the speed of light. At the second phase modulator output (point D), the field has been further modulated as $E_D(t) = \cos(\omega(t - dn/c) + \alpha(f_1(t - dn/c) + f_2(t)))$. It is easy to appreciate that, if the drive signals are configured such that $f_2(t) = -f_1(t - dn/c)$, then the two modulations cancel and the original narrowband linewidth is recovered, $E_D(t) = \cos(\omega t)$. Note that this reversible linewidth broadening occurs only when the delay of the signal f_2 relative to f_1 matches the optical group delay between the modulators.

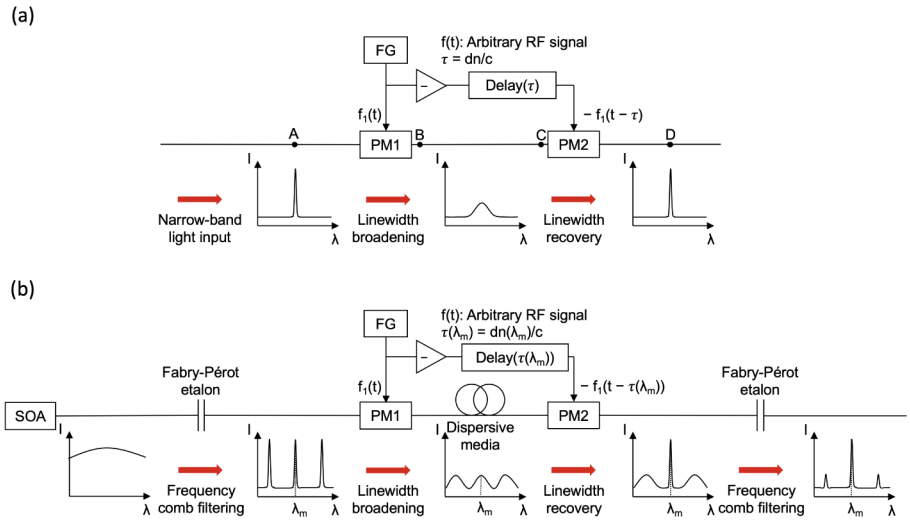

Fig. 1. Operating principle of phase code wavelength filter. (a) Linewidth broadening and recovery of narrow-band light by phase modulation and compensation. (b) Wavelength filtering using selective linewidth recovery of a frequency comb and Fabry-Pérot etalon by using dispersion between two phase modulators. PM, phase modulator; FG, function generator; SOA, semiconductor optical amplifier.

Biomedical Optics EXPRESS

In Fig. 1(b), we construct a combline transmission filter based on this principle of reversible linewidth broadening. Here, we add identical Fabry-Pérot etalons before and after the phase modulators and add dispersive fiber between the modulators. If we launch broadband (e.g., amplified spontaneous emission (ASE)) light, a frequency comb will be generated by the first etalon. Each line of this frequency comb will be equivalently broadened by the first phase modulator. Now, because of the dispersive fiber, each of the optical comblines experiences a different group delay in transit to the second modulator. The second modulator drive signal f_2 can be delayed such that it reverses the linewidth broadening for only one of the comblines ($f_2(t) = -f_1(t - dn(\lambda_m)/c)$). The output Fabry-Pérot etalon (identical to the first) then attenuates the optical power of the broadened comblines, while efficiently transmitting the single, narrow combline. By controlling the drive signal provided to the second modulator, any of the comblines can be selected for high transmission. Extending on this concept, a dynamic sequence of combline transmissions can be generated by applying an appropriately constructed drive signal to the second phase modulator. This dynamic combline transmission filter can then be used to create a stepped frequency comb laser.

3. Experimental design and operation of a prototype PCML laser

3.1. Laser architecture

To construct a laser, this electronically controlled phase-code filter was placed within a ring cavity (Fig. 2(a)). In this cavity, light travels from the output of the filter to the input of the filter without experiencing significant phase/spectral modulation. As a result, the two Fabry-Pérot etalons used in the filter (Fig. 1(b)) are redundant, and can be replaced by a single etalon. A fixed 80 GHz free spectral range (FSR) Fabry-Pérot etalon (Light Machinery) with a Finesse of 100 was used. The phase code filter included two lithium-niobate phase modulators (Covega) with 10 GHz RF bandwidth. An arbitrary waveform generator (Euvis, AWG872) provided the drive signals to these modulators through RF amplifiers. A dispersion compensating fiber (OFS, WBDK:84C-L) provided -84 ps/nm dispersion at 1550 nm between the phase modulators. To equalize the overall cavity roundtrip time across wavelengths (dispersion matching), an approximately 2.4 km length of SMF-28e+ was inserted in the cavity in double-pass configuration using a Faraday rotator mirror (FRM). The FRM eliminated the polarization mode dispersion of the SMF-28e+ fiber. A semiconductor optical amplifier (SOA, Covega) was located inside the cavity for amplification, followed by an 80/20 output coupler.

3.2. Driving waveforms

The drive waveforms provided to the first and second phase modulators set the filter transmission properties across time. Once the first modulator waveform was defined, the waveform for the second was found by applying the appropriate delay relative to the inverted first waveform. There are many waveforms that can be used to drive the first modulator. Here, we used a chirped sinusoid as the basis function for the first modulator waveform. The rationale was that a chirped sinusoid lacks a dominant frequency component. Dominant frequencies would create a periodicity in the delay response (i.e., autocorrelation function), which could allow multiple comblines to be transmitted through the filter.

For the first modulator, we constructed a repeating waveform to provide to the first modulator ($f_1(t)$). This waveform was constructed by concatenating a sinusoid that was chirped from 1.0 GHz to 1.9 GHz, or from 1.2 GHz to 2.3 GHz. Each chirping was performed over a duration t_p where t_p is the desired output pulsewidth (the time during which the laser output remains fixed at a given optical frequency). The chirped sinusoid was repeated indefinitely at the first modulator such that each output pulse was "encoded" with the same phase-modulation.

Biomedical Optics EXPRESS

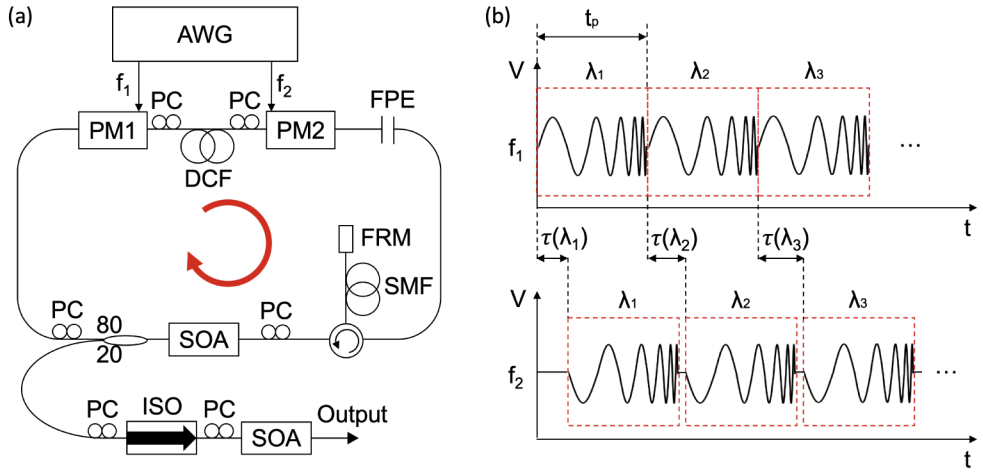

Fig. 2. (a) PCML laser setup. (b) Illustration of RF waveform design for phase modulators. AWG, arbitrary waveform generator; PM, phase modulator; PC, polarization controller; FPE, Fabry-Pérot etalon; DCF, dispersion compensating fiber; FRM, Faraday rotating mirror; SMF, single mode fiber; SOA, semiconductor optical amplifier; ISO, isolator.

The waveform provided to the second modulator was then constructed by concatenating sections of the chirped sinusoids that were used to form the first waveform. These chirped sinusoids were inverted, and delayed based on the desired output wavelength sequence. More specifically, the laser output combline frequency sequence was first defined. Next, a table of optical group delays for each optical combline frequency in this sequence was calculated. Finally, these delays were used to construct the second phase modulator drive signal as described above. Interpolation was used to connect the chirped sinusoid waveforms (Fig. 2(b)). With -84 ps/nm of dispersion between the modulators, the optical group delay difference between adjacent comblines (80 GHz free spectral range) was approximately 54 ps. Because this is significantly smaller than the arbitrary waveform generator clock cycle (125 ps), the digital representations of the chirped sinusoid were phase-shifted to induce delays with sub-clock cycle precision. Both the first and second modulator waveforms were designed such that the combline transmission filter was operated in resonance with the cavity roundtrip time, similar to the operation of Fourier-domain mode-locking.

4. Prototype PCML laser performance

4.1. Phase-code filter performance

Before building the prototype PCML laser, we first characterized the performance of the phase-code filter in isolation, i.e., outside of its integration into a laser cavity. This was done using the setup shown in Fig. 1(b). Amplified spontaneous emission (ASE) light was used as an input from an SOA. This light was transmitted through an 80 GHz Fabry-Pérot etalon with a finesse of approximately 100. A second, identical etalon was placed at the output and angle-tuned to align its comblines to those of the first etalon. Using an optical spectrum analyzer (Yokogawa, AQ6370C), we characterized the linewidth of each combline as they passed through the filter. Linewidths below 0.02 nm could not be resolved due to resolution limitations of the OSA. In the measurements shown in Fig. 3, the second modulator waveform was configured to decode the combline at 1560 nm. Note that all input comblines were equally broadened by the first phase modulator (Fig. 3(b)), but only the combline at 1560 nm was substantially narrowed after the second phase modulator(Fig. 3(c)). Next, we measured the transmission efficiency of

Biomedical Optics EXPRESS

each combline using the OSA. As expected, the narrowed combline was transmitted with high efficiency (Fig. 3(h)). The filter extinction for the other lines was greater than 3.5 dB (Fig. 3(h)).

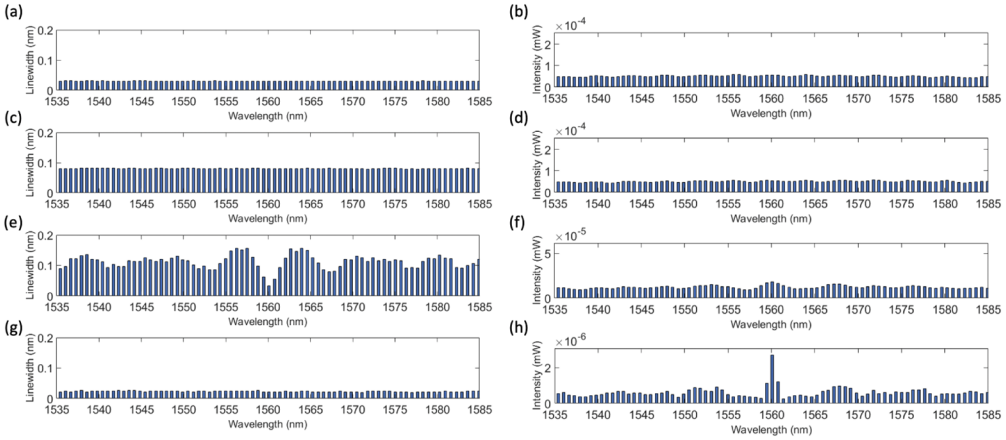

Fig. 3. Single-pass phase-code filter performance measurements of each combline. Linewidth (a, c, e, g) and intensity (b, d, f, h) were measured after passing the first etalon (a,b); after linewidth broadening by the first modulator (c,d); after linewidth recovery by the second modulator (e,f); and after filtering by the second etalon (g,h).

Biomedical Optics EXPRESS

4.2. PCML laser performance

Next we incorporated the filter into a ring cavity as shown in Fig. 2 and operated at three speeds: 176 kHz (5th harmonic of the cavity), 881 kHz (25th harmonic), and 3.52 MHz (100th harmonic). Figure 4 demonstrates the lasing spectra and time traces of the PCML laser in each of these configurations. At 176 kHz, a pulsewidth of 43 ns was used. At 881 kHz, a pulsewidth of 8.6 ns was used. For both these speeds, the laser output spanned 80 nm at 80 GHz combline spacing. In this prototype laser using the 8 GSPS AWG, we were not able to achieve consistent performance with pulsewidths below 8.6 ns. To achieve 3.52 MHz speeds while maintaining 8.6 ns pulsewidths, we reduced the number of output wavelengths by designing the waveforms to transmit every 4th combline. Note that these changes to laser performance required changes only to the AWG drive signals provided to the phase modulators; no hardware modifications were required. This enables a CR-OCT source that was widely tunable and rapidly re-configurable.

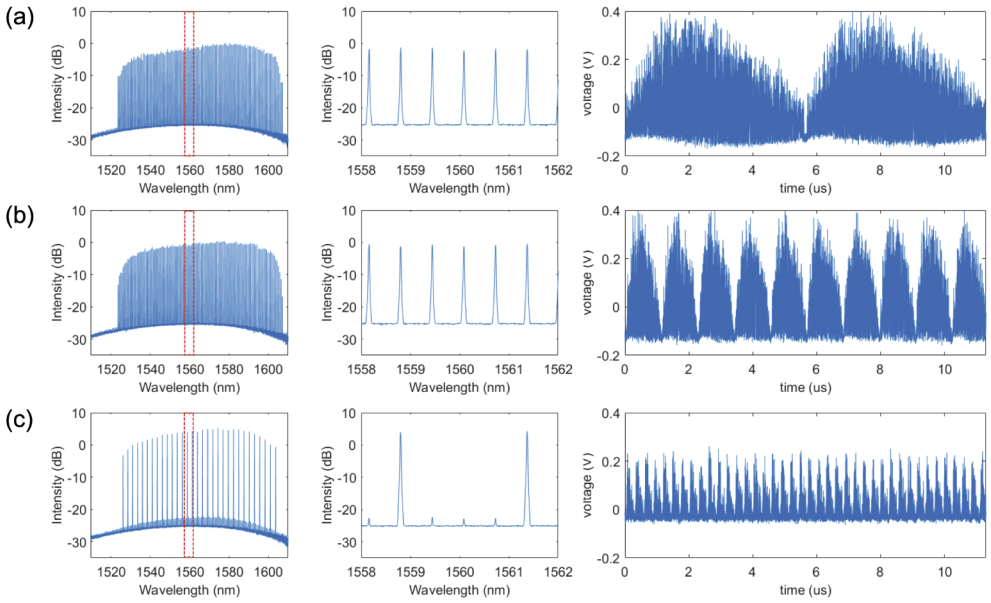

Fig. 4. Laser spectra (left), spectra in the wavelength range indicated by the red box on the left (middle), and the time trace (right) of the PCML laser operating at: (a) 176 kHz, 130 wavelengths, $t_p = 43\ ns$; (b) 881 kHz, 130 wavelengths, $t_p = 8.6\ ns$; and (c) 3.52 MHz, 31 wavelengths, $t_p = 8.6\ ns$.

Although the worst-case single pass extinction of the filter was approximately 3.5 dB, the laser output achieves a much higher comb line extinction due to the laser cavity resonance. The laser output spectrum illustrated in Fig. 4(c) suggests a spectral extinction in excess of 25 dB. However, when we consider that the selected lines have much lower duty cycles than the off-lines, the instantaneous laser extinction may be higher.

Biomedical Optics EXPRESS

The PCML laser coherence length was measured by acquiring fringe signals as a function of sample arm mirror position (relative to the reference arm). The measurement was done for 176 kHz and 881 kHz configurations for the analysis of the relationship between the pulse width and the coherence length of the source. The point-spread functions were calculated for fringe signals at the same circular delay position within increasing orders [5]. The axial resolution was measured from acquired point spread functions to be 17 μm, which was consistent with and without the booster SOA. The coherence length (6 dB roll-off) was 85 mm (mirror displacement) for pulsewidths of 43 ns (176 kHz A-line) and 8.6 ns (881 kHz A-line) (Fig. 5(a,c)). This would enable a 170 mm imaging range using circular-ranging with in-phase and quadrature fringe signal detection that discriminates between the positive and negative delay space. Note that the coherence length was measured to be the same for both pulsewidths. We would not anticipate that the coherence length would be affected by changing the sequence of output comblines at the same pulsewidth (e.g., 881 kHz and 3.52 MHz outputs), but we did not measure this explicitly. Because the prototype laser output power was low (approximately 1 mW), we also tested the PCML coherence length with a booster SOA (outside of cavity). The booster SOA increased power to 50 mW and decreased the coherence length to 50 mm (100 mm CR-OCT imaging range), as shown in Fig. 5(b,d). This reduction is a consequence of linewidth broadening in the SOA. We also observed that the booster SOA increased the noise floor, which needs to be examined further.

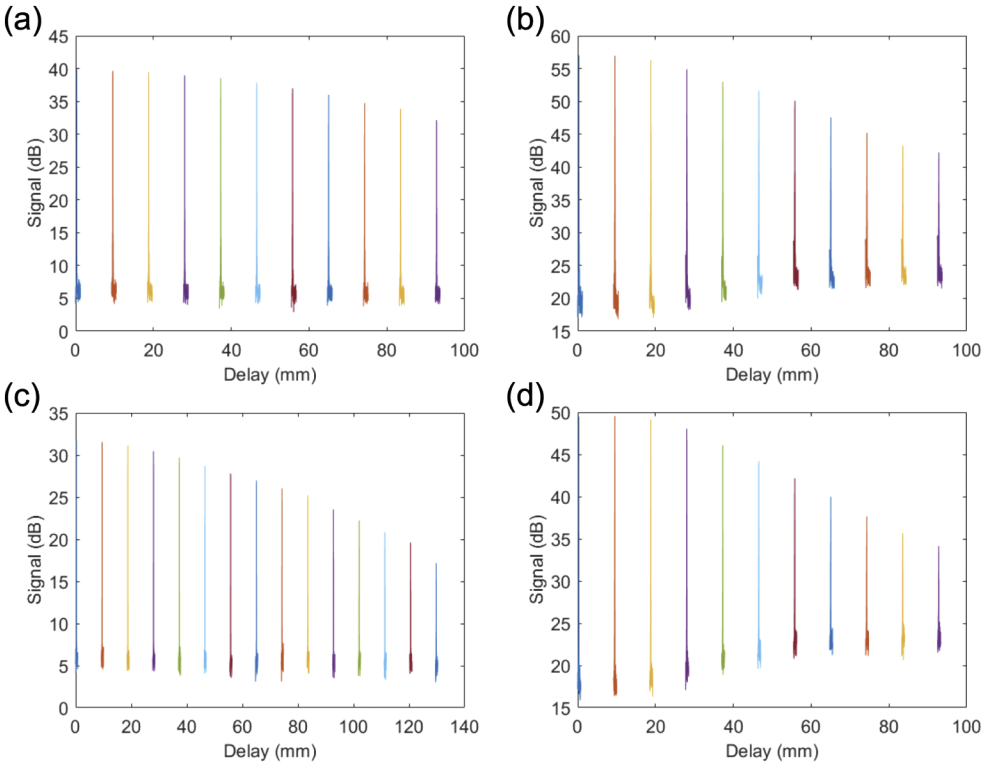

Fig. 5. 6 dB roll-off measurement of PCML laser operating at (a) 176 kHz without booster SOA, (b) 176 kHz with booster SOA, (c) 881 kHz without booster SOA, and (d) 881 kHz with booster SOA.

Biomedical Optics EXPRESS

4.3. CR-OCT imaging using the PCML laser

We acquired CR-OCT images at each of the three imaging speeds (176 kHz, 881 kHz, and 3.52 MHz). As expected, the circular depth/delay range for the 3.52 MHz image is different than that for 176 kHz and 881 kHz due to the generation of a 320 GHz frequency comb rather than an 80 GHz frequency comb. The laser was used with the booster SOA for imaging experiments. A quadrature demodulation circuit described in Ref. [9] was used to create in-phase and quadrature fringes needed for CR-OCT. Output fringes were directed to balanced photoreceivers (Thorlabs, PDB465C) for detection. The digitizer (Signatec, PX14400) acquired the signal from the detectors at 250 MS/s, which was significantly higher than was required to capture the 8.6 ns (3.52 MHz and 881 kHz) and 43 ns (176 kHz) pulsewidths. Figure 6 shows the acquired CR-OCT images of an IR detection card and a finger at each lasing speed, with averaging over 25 adjacent cross sections. The depths of the circular ranges were approximately 1.9 mm for 176 kHz and 881 kHz configurations and 0.48 mm for 3.52 MHz configuration. Note that the total imaging depth range and the circular delay range are distinct parameters; signals can be acquired over the total imaging range, which is limited by the source coherence, but appear within a compressed image equal to the circular delay range (See Ref. [5]).

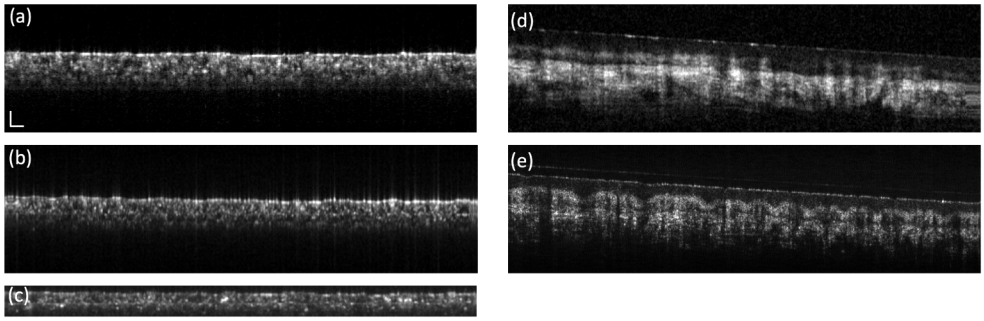

Fig. 6. Cross sectional images of (a-c) IR card and (d,e) finger with different A-line configurations with the same scales and corresponding circular ranges. (a,d) 176 kHz, (b,e) 881 kHz, and (c) 3.52 MHz. The dynamic ranges were (a,b) 20 dB, (c) 10 dB, and (d,e) 18 dB. Scale bar: 200 μm

5. Conclusion

In this work, we demonstrate a novel laser architecture providing stepped frequency comb outputs for moderate speed CR-OCT. In addition to enabling CR-OCT within the 100 kHz to several MHz speed range, the PCML laser design has several unique features. It was shown in the operation of the laser at 3.52 MHz that the PCML laser allows the user to set specific comblines, skip comblines, or modify the sequence of generated comblines. This was done through design of the drive waveforms, without hardware modification, and can be used to create highly re-configurable sources for CR-OCT. The speed of the PCML laser was not directly defined by the magnitude of the intra-cavity dispersion as is the case for SPML lasers. This allowed us to operate the PCML laser at much more moderate speeds. The upper speed limits of the PCML laser are not well-defined at this time. In principle, high-speed operation is possible. However, the high-bandwidth RF drive signals that would be required might be difficult to generate, and, at this time, the SPML architecture is likely more favorable for extremely high-speed operation. Additional advantages of the PCML architecture include a 100% duty cycle output and a linear-in-time output that does not require k-clocking or k-space resampling after digitization. Conversely, at present, the primary deficiency of the PCML laser is noise

Biomedical Optics EXPRESS

performance, which is significantly higher than mature OCT laser technologies. However, we do not believe that this noise is fundamental to the PCML approach, and we are currently working to understand the origin of the noise and demonstrate lower-noise PCML lasers.

Funding

National Institutes of Health (P41EB015903); Air Force Office of Scientific Research (FA9550-11-1-0331).

Disclosures

The authors declare no conflicts of interest.

References

1. S. H. Yun, G. J. Tearney, J. F. de Boer, N. Iftimia, and B. E. Bouma, "High-speed optical frequency domain imaging," Opt. Express **11**(22), 2953–2963 (2003).
2. M. A. Choma, M. V. Sarunic, C. Yang, and J. A. Izatt, "Sensitivity advantage of swept source and fourier domain optical coherence tomography," Opt. Express **11**(18), 2183–2189 (2003).
3. M. Siddiqui and B. J. Vakoc, "Optical-domain subsampling for data efficient depth ranging in fourier-domain optical coherence tomography," Opt. Express **20**(16), 17938–17951 (2012).
4. S. Tozburun, M. Siddiqui, and B. J. Vakoc, "A rapid, dispersion-based wavelength-stepped and wavelength-swept laser for optical coherence tomography," Opt. Express **22**(3), 3414–3424 (2014).
5. M. Siddiqui, A. S. Nam, S. Tozburun, N. Lippok, C. Blatter, and B. J. Vakoc, "High-speed optical coherence tomography by circular interferometric ranging," Nat. Photonics **12**(2), 111–116 (2018).
6. N. Lippok, M. Siddiqui, B. J. Vakoc, and B. E. Bouma, "Extended coherence length and depth ranging using a fourier-domain mode-locked frequency comb and circular interferometric ranging," Phys. Rev. Appl. **11**(1), 014018 (2019).
7. N. Lippok, B. E. Bouma, and B. J. Vakoc, "Stable multi-megahertz circular-ranging optical coherence tomography at 1.3 μm," Biomed. Opt. Express **11**(1), 174–185 (2020).
8. T.-H. Tsai, C. Zhou, D. C. Adler, and J. G. Fujimoto, "Frequency comb swept lasers," Opt. Express **17**(23), 21257–21270 (2009).
9. M. Siddiqui, S. Tozburun, E. Z. Zhang, and B. J. Vakoc, "Compensation of spectral and rf errors in swept-source oct for high extinction complex demodulation," Opt. Express **23**(5), 5508–5520 (2015).